Structure

Article

High-resolution cryo-EM analysis visualizes hydrated type I and IV pilus structures from enterotoxigenic *Escherichia coli*

Graphical abstract

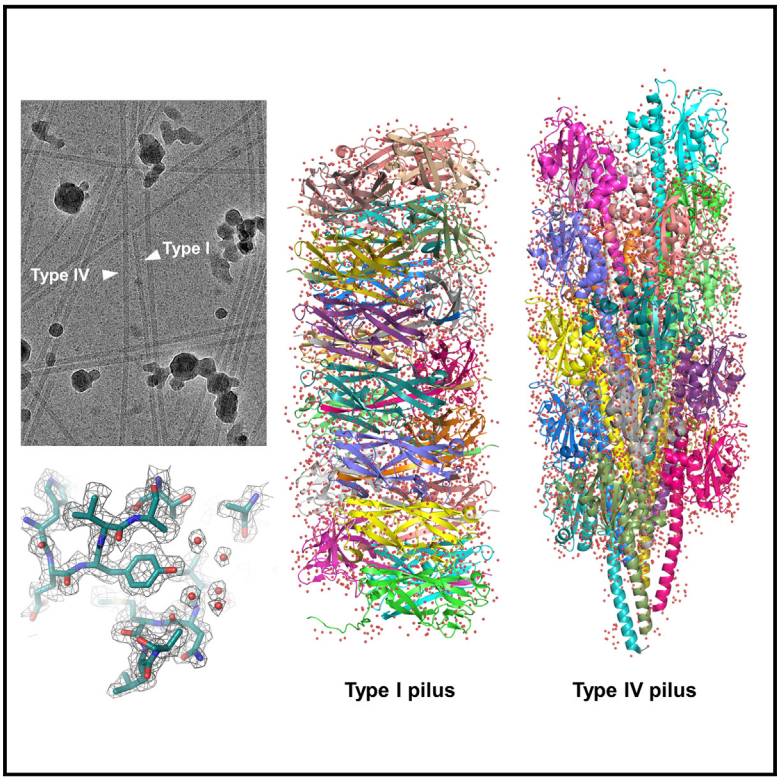

Authors

Kazuki Kawahara, Hiroya Oki, Minato Iimori, ..., Shigeaki Matsuda, Tetsuya Iida, Shota Nakamura

Correspondence

kkkazuki@phs.osaka-u.ac.jp (K.K.), nshota@gen-info.osaka-u.ac.jp (S.N.)

In brief

Kawahara et al. report near-atomic cryo-EM structures of type I and IV pili expressed in the enterotoxigenic *Escherichia coli* strain 31-10. The high-resolution cryo-EM structures provide insights into subunit-subunit interactions that advance our understanding of the biology of these pathogenetically important bacterial filaments, including pilus assembly, stability, and flexibility.

Highlights

- Cryo-EM structures of type I and IV pili expressed in enterotoxigenic *Escherichia coli*
- High-resolution maps facilitated the *de novo* structural modeling of type I and IV pili
- Water molecules were modeled around and within the inner core of the filaments
- Structures provide insights into pilus assembly, stability, and flexibility

Kawahara et al., 2025, Structure *33*, 1040–1050
June 5, 2025
https://doi.org/10.1016/j.str.2025.03.010

CellPress

CellPress

Structure

Article

High-resolution cryo-EM analysis visualizes hydrated type I and IV pilus structures from enterotoxigenic *Escherichia coli*

Kazuki Kawahara,[1,2,8,*] Hiroya Oki,[3,8] Minato Iimori,[1] Ryuki Muramoto,[1] Tomoya Imai,[4] Christoph Gerle,[5] Hideki Shigematsu,[6] Shigeaki Matsuda,[2,3] Tetsuya Iida,[2,3] and Shota Nakamura[2,3,7,9,*]

[1]Graduate School of Pharmaceutical Sciences, Osaka University, Suita, Osaka 565-0871, Japan
[2]Center for Infectious Disease Education and Research, Osaka University, Suita, Osaka 565-0871, Japan
[3]Research Institute for Microbial Diseases, Osaka University, Suita, Osaka 565-0871, Japan
[4]Research Institute for Sustainable Humanosphere, Kyoto University, Uji, Kyoto 611-0011, Japan
[5]Life Science Research Infrastructure Group, RIKEN SPring-8 Center, Sayo, Hyogo 679-5148, Japan
[6]Structural Biology Division, Japan Synchrotron Radiation Research Institute, SPring-8 Center, Sayo, Hyogo 679-5148, Japan
[7]Integrated Frontier Research for Medical Science Division, Institute for Open and Transdisciplinary Research Initiatives, Osaka University, Suita, Osaka 565-0871, Japan
[8]These authors contributed equally
[9]Lead contact
*Correspondence: kkkazuki@phs.osaka-u.ac.jp (K.K.), nshota@gen-info.osaka-u.ac.jp (S.N.)
https://doi.org/10.1016/j.str.2025.03.010

SUMMARY

Pathogenic bacteria utilize a variety of pilus filaments to colonize intestinal epithelia, including those synthesized by the chaperone-usher or type IV pilus assembly pathway. Despite the importance of these filaments as potential drug and vaccine targets, their large size and dynamic nature make high-resolution structure determination challenging. Here, we used cryo-electron microscopy (cryo-EM) and whole-genome sequencing to determine the structures of type I and IV pili expressed in enterotoxigenic *Escherichia coli*. Well-defined cryo-EM maps at resolutions of 2.2 and 1.8 Å for type I and IV pilus, respectively, facilitated the *de novo* structural modeling for these filaments, revealing side-chain structures in detail. We resolved thousands of hydrated water molecules around and within the inner core of the filaments, which stabilize the otherwise metastable quaternary subunit assembly. The high-resolution structures offer novel insights into subunit-subunit interactions, and provide important clues to understand pilus assembly, stability, and flexibility.

INTRODUCTION

Enteric bacterial pathogens have evolved numerous surface organelles to efficiently colonize their host environment.[1,2] Most of these organelles are filamentous protein polymers termed pili or fimbriae, composed of thousands of subunits called pilins.[3] For enterotoxigenic *Escherichia coli* (ETEC), a major cause of diarrhea in travelers and children in developing countries, a variety of pilus filaments have been identified, most of which are colonization factors (CFs).[4] The CFs are categorized into either CF antigens (CFAs) or coli surface antigens and classified into two pilus types synthesized by distinct assembly mechanisms, chaperone-usher pilus (CUP) and type IV pilus (T4P) assembly pathways.[3–9] In the CUP assembly pathway, major and minor pilins are polymerized via the extensively studied "donor-strand exchange" mechanism, in which an incomplete immunoglobulin (Ig)-like fold of each pilin subunit is complemented by a donor strand provided by the N-terminal extension of an adjacent subunit.[3–5] Meanwhile, the T4P assembly pathway is substantially more complex than the CUP assembly pathway.[6–9] It involves envelope-spanning supramolecular machinery, consisting of multiple membrane proteins that function concertedly to incorporate pilin subunits, utilizing mechanisms that have yet to be fully understood.

As the CUP and T4P play crucial roles in bacterial infection, they are key targets in an era of increasing antibiotic resistance for developing novel vaccines and antiadhesive drugs against bacterial pathogens.[10–12] However, the large size and insoluble and non-crystallizing nature of these filaments pose challenges for the implementation of conventional high-resolution structural biology methods such as X-ray crystallography and nuclear magnetic resonance.[13,14] Therefore, structural characterization has been primarily confined to the pilus subunit level using either detergent-solubilized full-length pilins[6,9] or modified pilin constructs to improve protein solubility.[5] The filament structure was then constructed by docking these high-resolution monomeric structures into medium to low-resolution (4.0–15.0 Å)

density maps obtained by negative-stain or cryo-electron microscopy (cryo-EM) structural analyses.[15–21]

Owing to the technological advancements of cryo-EM, the resolution has recently been much improved.[14] Near-atomic resolution structures, even for bacterial filaments such as CUP and T4P, are beginning to be reported, providing new insights into the intact pilus structures for both pilus types.[22–25] Nevertheless, the dynamic and flexible natures of these filaments still limit the achievable resolution, and the EM density maps obtained in previous studies are insufficient to define the exact orientation of amino acid side chains or to locate solvent molecules. Thus, key biophysical features such as pilus assembly, stability, and flexibility remain to be elucidated.

Here, we determined the cryo-EM structures of CUP and T4P from wild-type ETEC strain 31-10 at resolutions of 2.2 and 1.8 Å, respectively, the highest-resolution structures reported to date for each pilus filament family. The quality of density maps enabled us to perform *de novo* structural determination of these filaments and reveal unprecedented atomistic details of subunit-subunit interactions involving thousands of hydrated water molecules during bacterial filament structural analysis. The high-resolution cryo-EM structures provide insights that enhance our understanding of the biology of CUP and T4P filaments, both of which play crucial roles in bacterial colonization and pathogenesis.

RESULTS

Purification of the filaments from ETEC strain 31-10

ETEC strain 31-10 cells were grown on a CFA agar plate for optimal expression of CFs.[26] We used culture conditions previously shown to be well suited for the efficient expression of CFA/III, one of the CFs belonging to a member of the type IVb subclass of T4P (T4bP), which is responsible for the ETEC adherence to intestinal epithelium.[27,28] The expressed filaments were sheared from the cells through vortexing and subsequently purified using techniques such as sucrose density gradient ultracentrifugation. Transmission electron microscopy (TEM) analysis of the purified filaments based on negative staining reveals one dominant filament type with a diameter of approximately 80 Å and highly flexible morphology (Figure S1), consistent with the characteristics observed for the CFA/III filament.[27,29,30]

Cryo-EM of the type IVb pilus from ETEC strain 31-10

In contrast to its negative-staining TEM images, the cryo-EM micrographs showed that the filament has an unexpectedly straight morphology (Figure 1A). The collected cryo-EM movies were processed and analyzed using CryoSPARC.[31] The 2D class averages of the filament segments showed a homogeneous class amenable to performing reconstruction at a resolution of 2.5 Å following the application of an asymmetric helical refinement (Figures 1A and S2). The symmetric parameters were then estimated, and one clear solution, with a rise of 8.01 Å and a twist of 94.63° was found. Subsequent helical reconstruction using these parameters resulted in a high-quality cryo-EM density map with 1.8 Å resolution (Figure 1B). The resolution was estimated using the "gold-standard" map:map Fourier shell correlation (FSC) criterion of 0.143 (Figure S3). This surprisingly high-resolution reconstruction differs markedly from the previous cryo-EM reconstructions of T4Ps, in which the substantial filament polymorphism severely limits the achievable resolution.[14]

The density map exhibited sufficient quality to construct a filament model *de novo* using the program ModelAngelo without requiring any sequence input (Figure 1C).[32] The estimated subunit sequence derived from the initial model was ~88% matched to the sequence of CofA, a major pilin subunit from CFA/III (GenBank code: BAB62897.1).[29] Subsequent use of the sequence information results in a full-length CofA model (208 residues) for each pilin subunit in the filament (Figures 1D and 1E). Strikingly, the resolution of the reconstructions enabled location of 4,175 water molecules distributed both at the inner and outer surface of the filament (Figures 1B and 1C). The density maps and images of the 2D class average did not show any evidence of incorporation of the CFA/III minor pilin, CofB, within the filament body. This observation is consistent with the notion that the minor pilin only localizes at the pilus tip and may transiently interact with the base of a growing filament to induce pilus retraction.[33]

Each CofA subunit in the filament adopts a typical αβ-roll pilin fold consisting of one ~50 residue long α helix (α1) embedded within a central five-stranded antiparallel β sheet (Figures 1D and 1E). CofA is one of the largest pilins reported to date and belongs to the type IVb (T4b) subclass.[34] T4b pilin shares a similar αβ-roll fold with pilins of the type IVa (T4a) subclass but is considerably different from those in the type IVc subclass, which only has an α1 consisting of 40–60 residues as a main structural motif.[23,35] The globular domain of T4b pilin (~180–200 residues) is generally larger than T4a pilin (~150–175 residues), which is attributed to its considerably long variable regions, i.e., αβ-loop and D-region[9] (Figures 1E and 1F).

The globular domain of CofA is well superposed onto the crystal structure of the N-terminal 28-residues truncated CofA (ΔN28-CofA) (Cα root-mean-square deviation [RMSD] of ~0.7 Å),[36] implying no noticeable conformational change required for filament assembly (Figure 1E). The structure also reveals that α1 forms a straight continuous helix similar to monomeric X-ray crystal structures of full-length T4aP major pilins,[15,37–39] but drastically different from the T4aP major pilin structures in the filament, where α1 is partially melted at the conserved helix breaking residues, including Gly14 and Pro22 (Figure 1G).[14,17–19,22,24] Although Pro22 is not conserved among T4b pilins, three glycines conserved at positions 11, 14, and 19, may contribute to α1 flexibility.[23] Noteworthy, the α1 of CofA is slightly bent at Gly19, which apparently optimizes the hydrophobic interactions among α1s at the filament core (Figure 1D).

In the filament, each subunit (S) has contacts with a total of six subunits, $S_{\pm1}$, $S_{\pm3}$, and $S_{\pm4}$, each along with a right-handed 1-start, a left-handed 3-start, and a right-handed 4-start helix, respectively, as observed in other T4P (Figure 2A). The filament is primarily stabilized by a helically arranged interactions of α1s, in which the hydrophobic N-terminal half of α1 (α1-N: residues 1 to 25) of each subunit (S) has intimate hydrophobic contacts with the α1-Ns of adjacent subunits ($S_{\pm1}$) and is also interdigitated by the middle part of the α1s of subunits (S_{-3} and S_{-4}) (Figures 2B and 2C). The hydrophobic interaction along the 1-start helix is a conserved feature of the T4P family filament and is critical for T4P stability by forming a hydrophobic filament core.

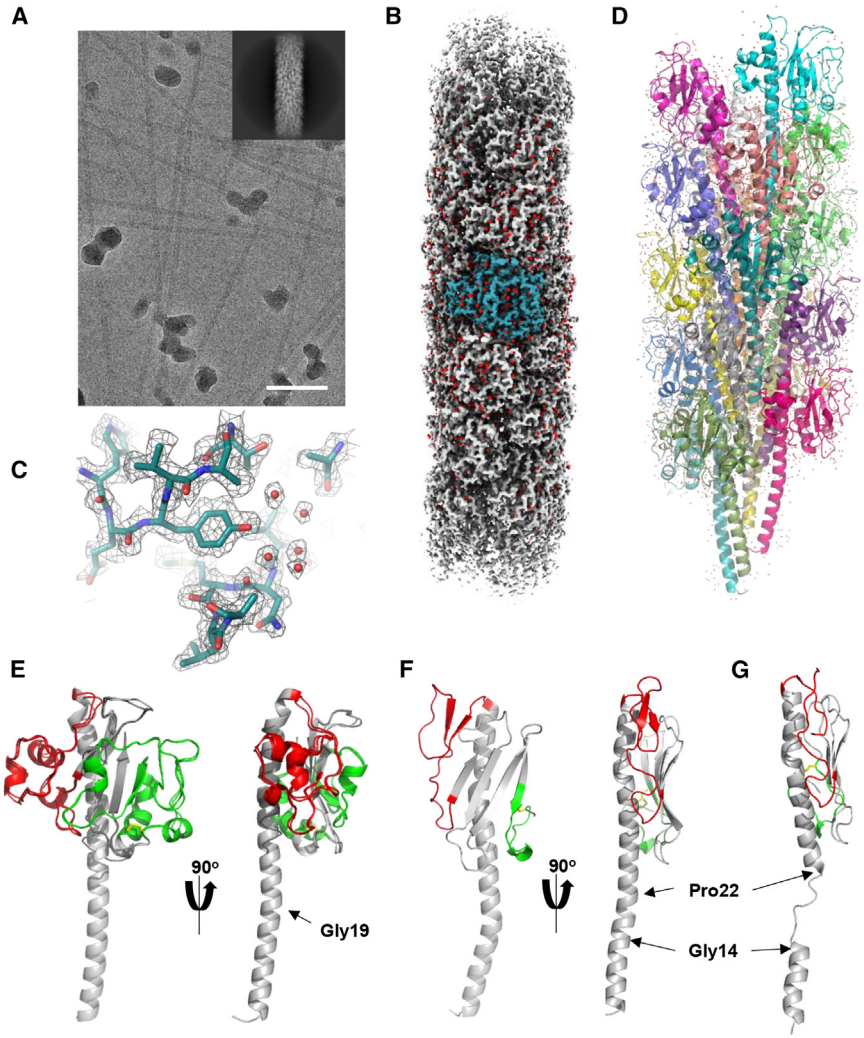

Figure 1. Cryo-EM structure of CFA/III from ETEC strain 31-10

(A) A representative example of a cryo-EM micrograph showing a highly straight filament with a diameter of 70–80 Å. A representative image of 2D class averages is shown in the inset. The scale bar represents 50 nm.

(B) The cryo-EM density map of the CofA filament. The densities corresponding to water molecules are colored in red. A part of the density map corresponding to one CofA subunit is shown in deep teal.

(C) A close-up view of the EM density map around Tyr145.

(D) Ribbon representation of the CofA filament model composed of 21 pilin subunits.

(E) Superposition of full-length structure of the CofA subunit in the filament (gray) and crystal structure of ΔN28-CofA (PDB code: 3VOR) (dark gray). The αβ-loop and D-region are colored in red and green, respectively. In CofA, the αβ-loop connecting α1 and the central β-sheet consists of residues 54 to 104, and the D-region located at the C terminus and stabilized by a Cys132-Cys196 disulfide bond consists of residues 132 to 196, surrounding the αβ core structure. The position of conserved Gly19 is indicated by a black arrow. The disulfide bond Cys132-Cys196 in the D-region is shown as a yellow stick model.

(F and G) Full-length structure of the major pilin PAK from *Pseudomonas aeruginosa* in crystal (F) or in filament (G) form (PDB code: 1OQW and 5VXY, respectively) as a representative example of T4a major pilin. The αβ-loop and D-region are colored in red and green, respectively. The positions of Gly14 and Pro22 are indicated by arrows. The disulfide bond Cys129-Cys142 in the D-region is shown as a yellow stick model.

Surprisingly, the intermolecular salt bridge between conserved Glu5 and the N-terminal amine of the adjacent subunit, which is proposed to be crucial in pilus assembly and stability,[7,17] is not observed. Instead, the side chain of Glu5 interacts with the backbone amide of Leu3 on the adjacent subunit S_{+1} (Figure 2D). The density map demonstrated that the N-terminal five residues adopt a turn-like conformation, in which Glu5 intramolecularly interacts with the N-terminal amine of Met1 (Figure 2E). The Glu5 residue also aids water-mediated interactions with two nearby Ser2 residues, and this relayed interaction further strengthens the α1-N interactions along the 1-start helix (Figure 2D). We found a water-filled gap (gap1) at the bottom of each α1-N (Figures 2B and 2C). The water molecules in gap1 form hydrogen-bonding networks that run helically through the inner groove of the otherwise hydrophobic filament core (Figures 2C and 3A). As also observed in a recent cryo-EM analysis of the actin filament,[40] the existence of a water channel in the filament not only helps to stabilize the hydrophilic interactions in the filament core but also may lubricate the mechanical rearrangements of subunits upon responding to external forces.

The amphipathic C-terminal half of α1 (α1-C: residues 25 to 51) of each subunit (S) is, on the other hand, surrounded by α1s of subunits S_{+3}, S_{+4}, and S_{+7} (Figures 2B and 2C). Although the α1-C (S) forms relatively loose contacts with the α1 of subunit S_{+4}, there is a notable gap (gap2) between α1-C (S) and the other two α1s of subunits S_{+3} and S_{+7} (Figures 2B and 2C). Gap2 is filled with water molecules that can communicate with water molecules in gap1 (Figures 3A and 3B). The gap water molecules are likely to function to buffer otherwise unstable α1 packing at this subpart of the filament core. Notably, these water-filled gaps are present right next to the middle part of α1 (at S_{-4} and alternatively at the S_{+3} position in Figures 2B and 3B) and are potentially capable of accommodating conformational changes of α1 (e.g., melting), when it occurs, as observed in other T4P filaments.[14,17–19,22,24]

Owing to the large molecular size of CofA, the filament surface is densely packed with each CofA globular domain (Figures 2A and 2F). However, only a few direct contacts involving a limited number of hydrogen bonds, salt bridges, and hydrophobic interactions are formed at each interacting interface ($S/S_{\pm1}$ or $S/S_{\pm3}$ or $S/S_{\pm4}$) (Figure 2G). The interfaces are instead filled with and stabilized by an extensive number of water-mediated hydrogen-bonding networks. The networking water molecules are distributed throughout the filament, enabling bulk water

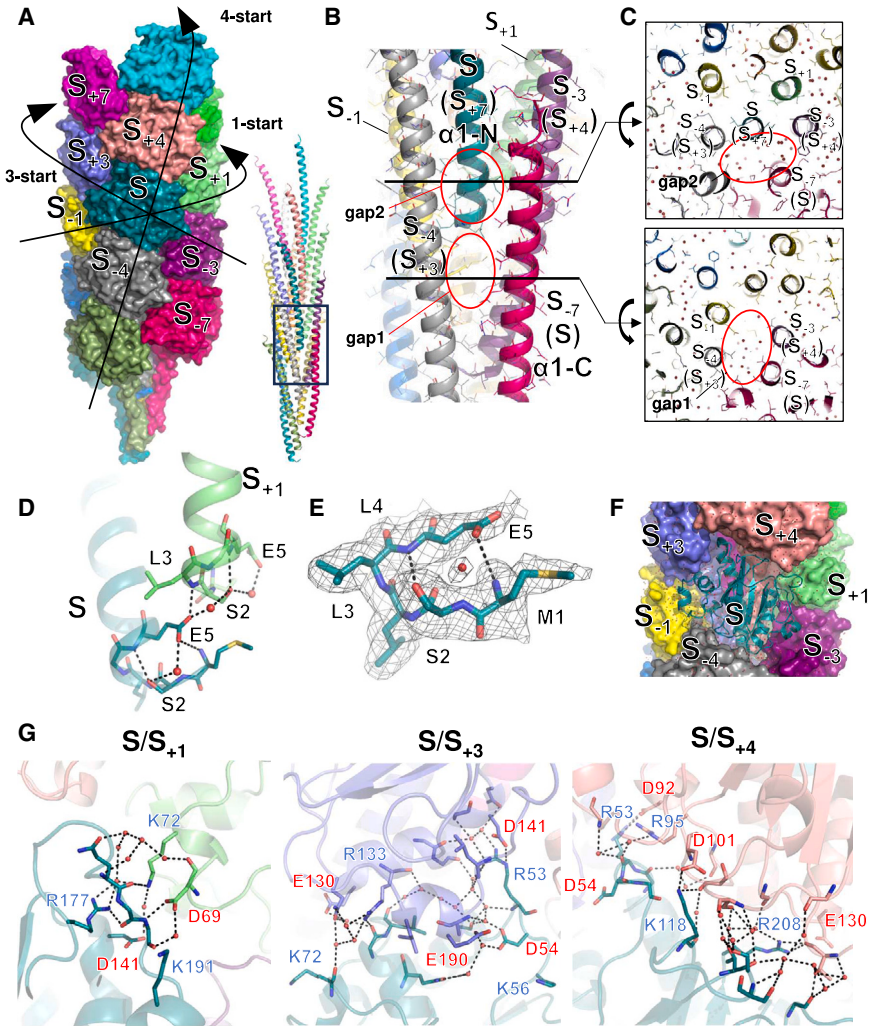

Figure 2. Subunit-subunit interactions in the CofA filament

(A) Surface representation of a CofA filament, where each subunit is colored differently (left panel). The subunit colored in deep teal is a reference and labeled as S. The remaining subunits are labeled along the 1-start helix. The directions of the subunits along the 1-, 3-, and 4-start helices are indicated by arrows. The ribbon representation of α1 interactions is also shown in the right panel.

(B) Close-up view of the α1 interactions. To describe the environment around α1-N, the position of each subunit is labeled, where one of the subunits colored in deep teal is taken as a reference (S). The labeling is also made by one of the subunits colored in magenta as a reference (S) to show the environment around α1-C and indicated in parentheses. Two gap regions are indicated by red circles.

(C) Two representative slices of the CofA filament at positions indicated in B, showing pools of water molecules at gap1 (bottom panel) and gap 2 (top panel) region.

(D) Close-up view of the N terminus interaction between subunit S and S_{+1} along the 1-start helix.

(E) EM density map of the N-terminal five residues of a subunit at S position contoured at the 2.0 RMSD level. The N-terminal residues are shown as stick models and labeled. A water molecule located between Glu5 and Ser2 is shown as a red sphere.

(F) Molecular packing around subunit S. Each CofA subunit (S) has contacts with a total of six CofA subunits ($S_{\pm1}$, $S_{\pm3}$, and $S_{\pm4}$).

(G) Interactions observed at the molecular interface between each pair of CofA subunits, S/S_{+1}, S/S_{+3}, and S/S_{+4}. For each CofA subunit, the residues involved in the interactions are shown as stick models and charged residues are labeled. Water molecules involved in the interaction networks are shown as red spheres.

to easily permeate into the filament core, especially via communication with water molecules in the two gap regions (Figures 3B–3D). Water accessibility is apparently affected by the packing of globular domains, dictated by the interactions between variable regions. In CofA, a long αβ-loop containing a characteristic 3/10-helix between α1 and α2 partly fills the interface between subunits (Figure 3C), thus making it narrower than the other T4P filaments, such as toxin coregulated pilus (TCP) from *Vibrio cholerae*, which have a relatively short αβ-loop that would intriguingly expose α1 (Figure S4).[18,23,41] In addition to the surface-localized hydrated water molecules, these interfacial water molecules could play an important role in pilus stability and flexibility.

Cryo-EM of the type I pilus from ETEC strain 31-10

In addition to CFA/III, we recognized another straight filament in the cryo-EM micrographs, which has a different morphology from T4P (Figure 4A). To characterize this filament, we segmented the corresponding filament images and performed iterative rounds of segment picking and 2D classification (Figure S5). The 2D class averages showed some features suggestive of CUP (Figures 4A and S5). We used several symmetrical parameters from previously reported structures of CUP as initial symmetric estimates and found a possible combination of an axial rise of 7.72 Å and a twist angle of 114.90°. Subsequent helical refinement using this parameter set leads to a well-defined density map at a resolution of 2.2 Å (Figure 4B). The resolution was estimated using the "gold-standard" map:map FSC criterion of 0.143, as shown in Figure S6.

The model was created *de novo* using the program ModelAngelo without any sequence input,[32] resulting in a filament model, in which each subunit consists of 158 amino acid residues. The BLASTp search using the estimated sequence showed an approximate 84% match to the sequences of type I fimbrial subunit protein FimA from *Shigella flexneri* and ETEC (GenBank code: UMV06456.1 and QED7455.1, respectively), suggesting that the observed CUP filament is a type I pilus (T1P).

Previous studies have focused on the plasmid-encoded CFs as possible surface-expressed bacterial filaments of ETEC. However, a recent study has pointed out that a wide variety of ETEC strains can express chromosome-encoded T1P as an important factor for intestinal colonization.[42] Since the existence

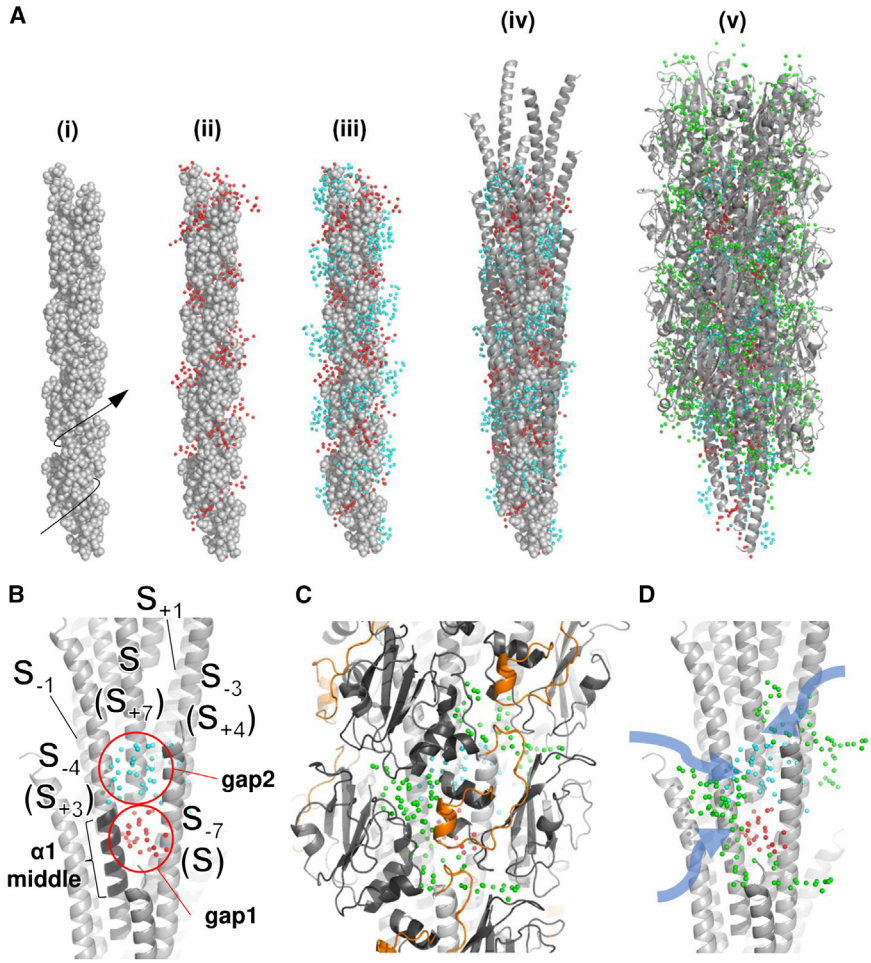

Figure 3. Hydration structure of the CofA filament

(A) Layers of water molecules in the CofA filament. The sphere representation of the hydrophobic filament core, formed by the interactions among each hydrophobic α1-N (6–16 residues) of the CofA subunit, shows a helically arranged inner groove (i). The inner groove shown by the arrow in the left panel is filled with water molecules (red-colored spheres) located in the gap1 region (ii). The gap2 water molecules (blue-colored spheres) helically cover the outer surface of the hydrophobic filament core (iii). The rest of the α1 (17–51 residues) and globular domains wrapped around the filament core, and the molecular interface of globular domains are filled with a substantial number of interfacial water molecules (green-colored spheres) (iv and v).

(B) An example of water distribution at two gap regions. Water molecules at gap1 and gap2 are colored in red and blue, respectively, and depicted as spheres. A middle region of α1 of one of the CofA subunits (S_{-4} or alternatively say S_{+3} in this case) next to the gap water molecules, is colored in black.

(C) An example of interfacial water molecules (green spheres) distributed around one subunit (S_{-7} or alternatively say S in this case). The loop containing a characteristic 3/10-helix between α1 and α2 found in CofA, which partly fills the molecular interface is colored in orange.

(D) Possible access routes for bulk water to reach into the filament core via communication with water molecules at two gap regions.

of *fimA* and its associated genes had not yet been examined for ETEC strain 31-10, we determined the whole genome sequence of the strain and identified T1P-related genes (Figures 5A and 5B). The FimA sequence was then used for subsequent modeling that resulted in a full-length model of FimA, except for the N-terminal disordered Thr1, confirming further that the observed filament expressed in ETEC strain 31-10 is T1P (Figure 4C).

The structure of FimA filament is essentially the same as the previously determined cryo-EM structure of T1P from uropathogenic *E. coli* (UPEC).[20] Each FimA subunit in the filament adopts an incomplete Ig-like fold, which lacks the C-terminal β strand that is complemented by the N-terminal donor β strand of the adjacent subunit (Figure 4D).[5,20] In addition to this complemented interaction between subunits ($S/S_{\pm1}$) involving mostly hydrophobic interactions, each subunit (S) primarily forms additional contacts with a total of four subunits, $S_{\pm2}$, and $S_{\pm3}$, to form a rod-like pilus filament. As expected from their high sequence similarity (91% identity) between the FimA subunit of ETEC and UPEC, almost all of the residues involved in subunit-subunit interactions were conserved. The variable residues were principally observed on the exterior surface of the FimA subunit, which is indicative of immune pressures selecting for antigenic diversification (Figure S7).[21]

The highest-resolution structure for T1P shows that the largest subunit-subunit interactions at the $S/S_{\pm3}$ interface involving many charged residues located at each of the complementary charged patches, which is thought to be important for the formation of the helical quaternary structure (Figures 4E and S8).[20,21,25] However, although they are each located close, most of these charged residues do not form salt bridges. These residues include Asp64 and Asp116 (corresponding to Asp62 and Asp114, respectively, in FimA from UPEC), which are proposed to be important in pilus stability by mutational analysis.[21] As in the case of the CFA/III filament, the subunit-subunit interface is filled with an extensive number of water molecules, stabilized by the water-mediated hydrogen-bonding networks (Figure 4F).

DISCUSSION

Recent advances in cryo-EM and cryo-electron tomography have emerged as powerful tools for identifying and determining the structure of bacterial filaments expressed in response to various types of environmental cues. As demonstrated in this study, high-resolution cryo-EM can determine the filament structures of T1P and T4P *de novo* at near-atomic levels. This capability enhances our understanding of the pilus biology of these filaments, including assembly, stability, and flexibility,

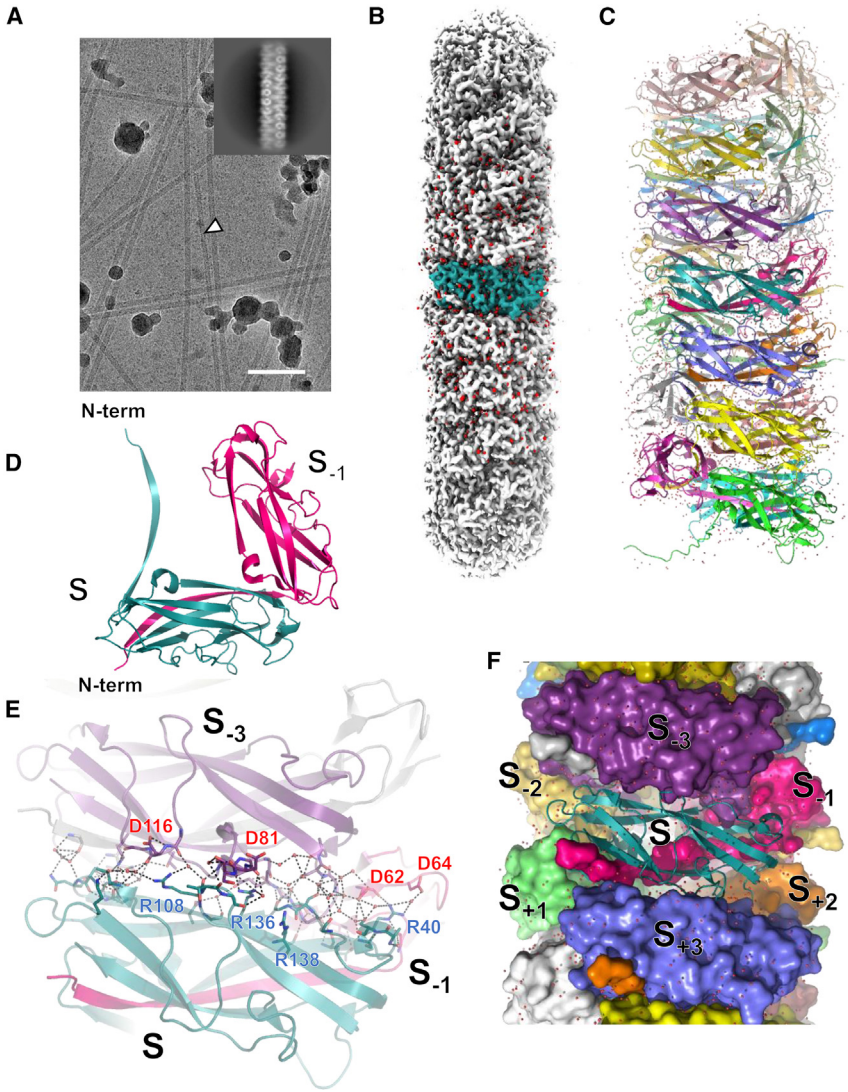

Figure 4. Cryo-EM structure of the type I pilus from ETEC strain 31-10

(A) An example of a cryo-EM micrograph showing the existence of a relatively thin (~70 Å) filament, which is morphologically different from CFA/III. The filament is indicated by a white arrowhead in the micrograph. A representative image of 2D class averages of the filament showing a feature of T1P is shown in the inset. The scale bar represents 50 nm.

(B) The cryo-EM density map of the FimA filament from ETEC strain 31-10. The densities of water molecules are colored in red. A part of the map corresponding to one pilin subunit is shown in deep teal.

(C) Ribbon representation of the FimA filament model composing 21 pilin subunits.

(D) Subunit interaction between subunits S (colored in deep teal) and S_{-1} (colored in magenta). The N-terminal donor strand of one subunit (S_{-1}) is inserted into the hydrophobic groove of the neighboring subunit (S) by the so-called "donor-strand exchange" mechanism.

(E) Subunit interaction between subunits S and S_{-3}, colored in deep teal and purple, respectively. The residues involved in the interactions are shown as stick models and charged residues are labeled. Water molecules involved in the interaction networks are shown as red spheres.

(F) Molecular packing around subunit S. Each FimA subunit (S) has contacts with a total of six FimA subunits ($S_{\pm1}$, $S_{\pm2}$, and $S_{\pm3}$).

which are important for efficient infection by pathogenetic bacteria.

Although pilus assembly mechanisms have been well characterized for T1P,[3,5] those for T4P have not yet been fully elucidated.[8] This is partly attributed to the partial melting of α1 observed in almost all of the reported T4P structures that limits the resolution of structural analysis and also prevents the elucidation of the initial subunit docking process at the inner membrane, where α1 could form a continuous helix. The CFA/III structure reported here with a continuous α1 thus may infer the mechanism of such a process. The structure suggests that each pilin subunit is added to the base of the growing pilus by simple docking (Figure 6Aii–6Aiv). The concave binding surface, composed of subunits S_{+1}, S_{+3}, S_{+4}, and S_{+7}, of the growing pilus well accommodates the incoming subunit, S, without forcing any conformational changes, even if it has a large globular domain like CofA (Figure 1E). Docking is primarily driven by the long-range electrostatic interactions between each pair of charged residues located in a total of six oppositely charged surface patches (Figures 2G and 6B).

It has been proposed that complementarity between a conserved, negatively charged Glu5 of the incoming subunit and a positively charged N-terminal amine of the terminal subunit in a growing pilus is a possible driving force for the docking.[7,17] However, our high-resolution structure unambiguously reveals that Glu5 interacts with the backbone amide of Leu3 in the neighboring subunit (S_{+1}) and intramolecularly neutralizes the N-terminal amine, by which the N-terminal five residues adopt a turn-like conformation (Figure 2E). This turn-like conformation, in which Glu5 is positioned close to the N-terminal amine, has been observed in the crystal structures of monomeric T4a major pilins.[15,38] Although a similar conformation has been modeled in three recently reported cryo-EM structures of T4aPs (one from *Myxococcus xanthus* and two from *Thermus thermophilus*, determined at 3.0–3.5 Å resolution),[22,24] no such neutralization interaction has been experimentally confirmed in the filament structure, likely owing to the limited resolution of the maps (Figure S9). Notably, the intramolecular Glu5-Met1 interaction observed in the CofA structure is suited for their transition to the acyl phase of the membrane. However, as they are initially responsible for anchoring α1 to the inner membrane by interacting with lipid head groups, the question arises regarding the formation of this conformation after the signal sequence cleavage. To obtain some insight, we constructed an AlphaFold-modeled structure of a major pilin-prepilin peptidase complex that showed that the corresponding N-terminal region should be unwound to

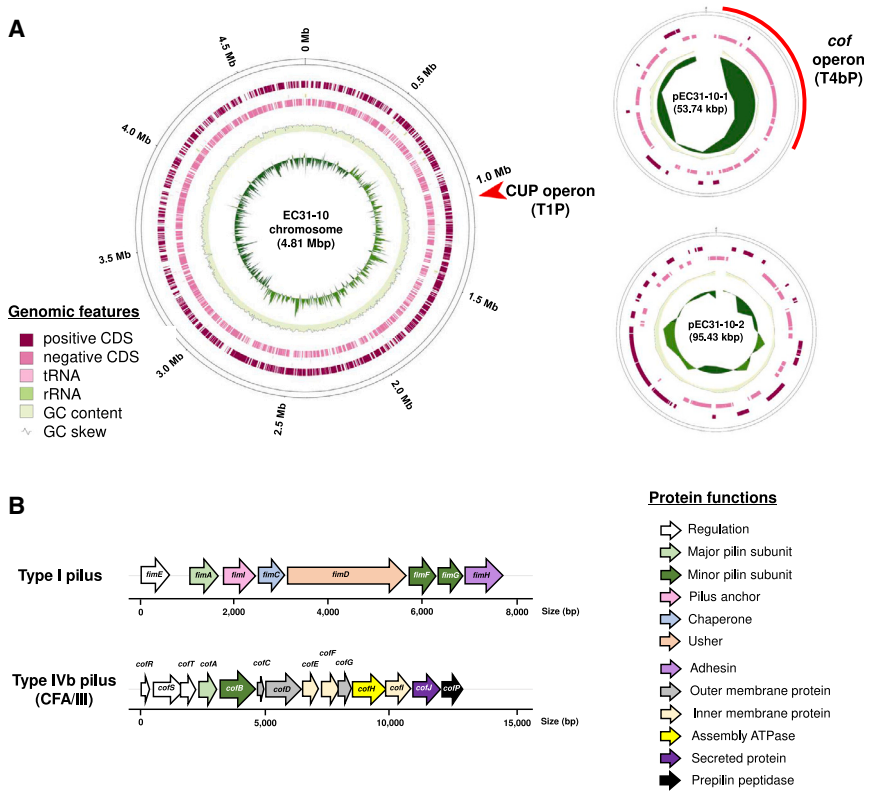

Figure 5. Whole genome sequencing of ETEC strain 31-10

(A) The genome of ETEC strain 31-10 visualized using GenoVi[43] (not to scale). The red arrow and arc indicate the position of operons involved in the pili formation of type I and type IVb pilus (CFA/III). (B) Gene-cluster of the type I and type IVb pilus (CFA/III) (left panel). Each gene is color-coded based on the predicted function of the protein. Predicted protein functions for each gene product are shown at the right panel.

interact with the peptidase active site (Figures 6Ai and S10). We thus speculate that upon cleavage of the signal sequence, the N-terminal region maintains its unwound conformation by forming a turn-like structure and acts as a trigger to transfer the N terminus of α1 from the cytoplasm to the acyl phase of the membrane with the help of a cytoplasmic assembly ATPase and/or platform proteins[8,45,46] (Figure 6Aiii–6Av).

As mentioned earlier, surface charge complementarity is important for a long-range attraction of pilus docking, and many residue pairs with opposite charges are found at each subunit interface (Figure 6B). However, most of these charged residues do not form salt bridges (Figure 2G). Surprisingly, we recognized only a few direct interactions among residues and found that the interface is filled with an extensive number of water-mediated networks (Figures 2G and 6C). This also applies to T1P, in which the largest subunit–subunit interface, $S/S_{\pm3}$, was dictated by suboptimal electrostatic and water-mediated interactions (Figures 4E and 4F). Although the hydrophobic N-terminal interactions consolidate the filament assembly in both pilus types, these non-specific water-mediated interactions among their globular domains are "metastable" and sensitive to external forces, and could play important roles in pilus dynamics, e.g., an assembly or disassembly (retraction), an extension or bending of T4P,[47,48] and a coil-uncoil reaction of T1P,[21,25] where water molecules play a lubricating role (Figure 6D).

In T4P, this suboptimal interaction is partly attributed to a surface mismatch between the hydrophilic surface of α1-C of incoming subunit (S) and the hydrophobic patch composed of α1-Ns of subunits (S_{+3}, S_{+4}, and S_{+7}) at the pilus base (Figure S11). This creates gaps (gap1 and gap2) among subunits that can be filled with water molecules (Figures 2 and 3). As seen in the previously reported T4aP cryo-EM structures,[14,17–19,22,24] the gaps may function as a compression space that accommodates the melting portion of the nearest α1 (Figure 3B), when responding to external forces such as shear forces *in vivo* and blotting forces during cryo-EM grid preparation.[25,49] The susceptibility to such forces apparently depends on the strength of the interactions among globular domains at the filament surface.[24] Thus, filaments composed of pilin subunits with a larger globular domain and longer variable regions would tend to be more tolerant against forces than those composed of smaller ones, as demonstrated here in the CFA/III filament.

The local resolution map of CFA/III intriguingly shows that the resolution on the filament surface is comparable to that in the interior, suggesting the rigidity of the surface exposed globular domains (Figure S12). This feature is also observed in T1P, which has a relatively large globular domain among CUP family filaments (Figure S13).[25] Given that the water molecules at the subunit interfaces are trapped under cryogenic conditions and contribute to freezing the mobility of protein atoms around them, we thus envision that the "solvent slaving" effect,[50] coupled with densely packed pilins, consolidates the filament and leads to the highest-resolution cryo-EM structures reported to date for each of the pilus types. In CFA/III, it should be noted that the resolution of the middle of α1, including Gly11, Gly14, and Gly19, conserved in the T4bP family, is lower than the others, suggesting potential flexibility (Figure S12). Considering the lubricating role of hydrated water molecules, the filament can be flexible at room or higher temperatures, as captured by its negatively stained TEM images (Figure S1).[27,29,30]

Recently, a cryo-EM structure of another T4bP, TCP from *V. cholerae*, was reported at 3.8 Å resolution.[23] Notably, the cryo-EM images of TCP show a highly flexible and wavy nature, contrasting with the straight morphology of CFA/III. The TCP filament was reconstructed in a bending conformation, where some of the α1s are partially unwound at the region containing Gly11, Gly14, and Gly19, and the $S/S_{\pm1}$ and $S/S_{\pm4}$ interfaces are disrupted. Although the major pilins of these two T4bP variants share a similar overall protein fold, a notable difference is observed in

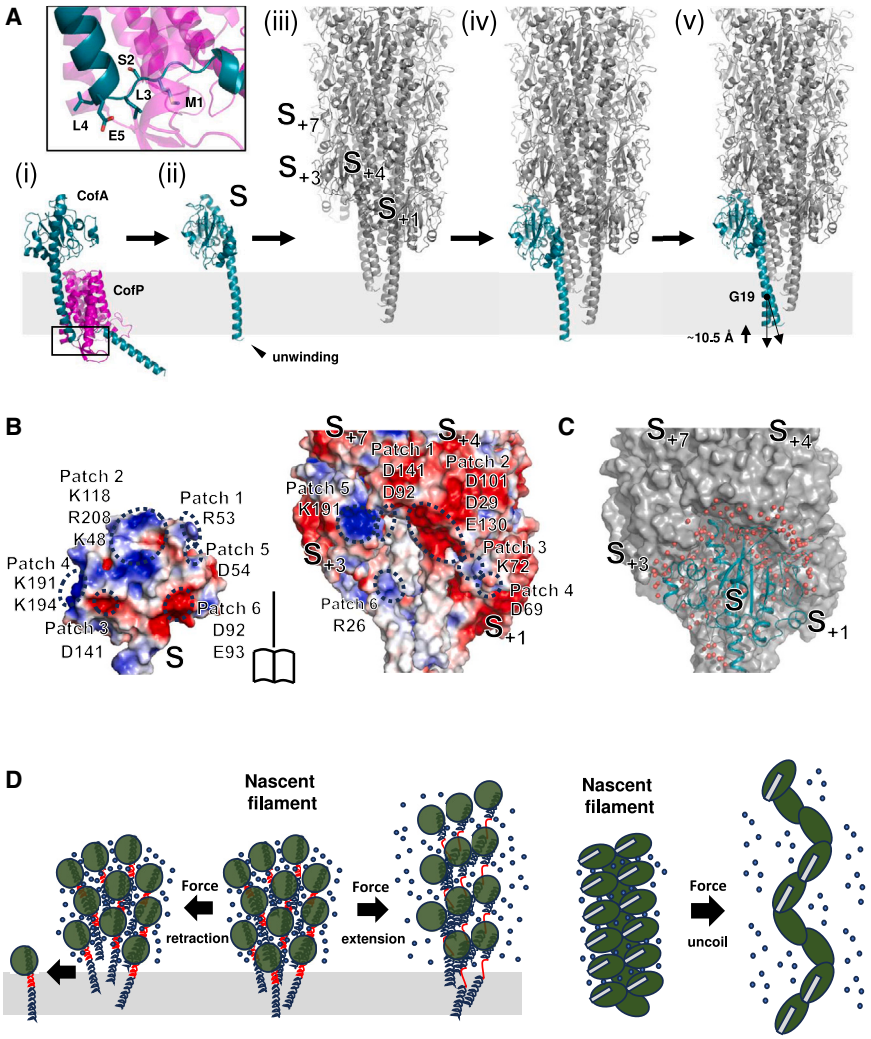

Figure 6. Proposed mechanism of subunit docking in the growing T4bP filament

(A) A schematic representation of the initial subunit docking process at the inner membrane. After the major pilin subunit is recognized by prepilin peptidase with its N-terminal region (residues 1–5 of matured pilin) partially unwound (i), the type III secretion signal is cleaved off, and the N-terminal five residues may remain unwound and take a turn-like conformation, in which positively charged N-terminal amine is neutralized by the interaction with negatively charged Glu5 (ii). The subunit is then docked onto the base of the growing pilus filament driven by long-range electrostatic interactions among their globular domains (iii and iv). Subsequently, the subunit is thrust up by ~10.5 Å via the function of a cytoplasmic assembly ATPase (v). As described in the main text, the neutralization of the N terminus lowers the energetic barrier of this extraction step of the major pilin, with the help of platform proteins. Once extracted, the α1 bends slightly to optimize the hydrophobic and hydrogen-bonding interactions among α1-Ns in the filament core, in which conserved Gly19 in T4b pilin (corresponding to Pro22 in T4a pilin) plays a pivotal role (v).

(B) Electrostatic surface complementarity between the incoming subunit (S) and the base of the growing pilus filament. The electrostatic surface potential was calculated by the Adaptive Poisson-Boltzmann Solver (APBS) program.[44] Each pair of oppositely charged patches is indicated by a dashed circle labeled from patch 1 to patch 6. The charged residues located at each patch are also labeled.

(C) Water molecules located at the interface between the incoming subunit (S) and the base of the growing pilus filament. The water molecules are shown as red spheres.

(D) Models of pilus conformational changes upon responding to external forces. Nascent T4P is metastable, in which each subunit interacts with each other through weak non-specific electrostatic interactions stabilized by interfacial water molecules, and easily dissociates or extends under the influence of external forces (left panel). The helically arranged T1P coil is uncoiled because of external forces, but the N-terminal mediated tight interaction between subunits connects each subunit and inhibits its dissociation (right panel).

their α/β-loop. Specifically, CofA uniquely possesses a 3/10-helix inserted between α1 and α2 (Figures 3C and S4). This insert fills the surface gap at the junction among subunits and stabilizes their globular domain interactions, particularly at the S/$S_{\pm1}$ and S/$S_{\pm4}$ interfaces, which are disrupted in the TCP filament (Figure S4).[23] This structural difference likely accounts for the variations in filament flexibility and the resolution of cryo-EM analysis observed between these two homologous T4bPs.

In summary, the high-resolution cryo-EM structures of CUP and T4P purified from ETEC strain 31-10 reveal that, in contrast to the stable hydrophobic filament cores, the interactions among globular domains are formed by rather weak electrostatic interactions stabilized by an extensive number of water molecules. The water molecules form a hydrogen-bonding network, distributed throughout the filament including even at the inner filament core, which play an important role in pilus assembly, stability, and flexibility. As bacterial filaments are crucial components for successful host infection, this structural information will be useful for drug discovery and vaccine development against enteric pathogens with multi-drug resistance.

RESOURCE AVAILABILITY

Lead contact

Further information and requests for resources and reagents should be directed to and will be fulfilled by the lead contact, Shota Nakamura (nshota@gen-info.osaka-u.ac.jp).

Materials availability

For any correspondence related to the materials used in this study, please contact the lead contact.

Data and code availability

The cryo-EM map and model of CFA/III have been deposited to EMDB and PDB, with codes EMD-60902 and 9IUF, respectively. The cryo-EM map and model of type I pilus have been deposited to EMDB and PDB, with codes EMD-60903 and 9IUG, respectively. The sequencing data of ETEC strain 31-10 have been deposited to DDBJ with an accession number of

PRJDB18453. They are publicly available as of the date of publication. Accession codes are also listed in the key resources table. This paper does not report original code. Any additional information required to reanalyze the data reported in this paper is available from the lead contact upon request.

ACKNOWLEDGMENTS

We thank Hiroki Tanino, Tomoko Miyata, and Keiichi Namba for assistance with cryo-EM data screening at Osaka University. Conventional TEM observations based on negative staining were performed in the Analysis and Development System of Advanced Materials (ADAM) collaborative research facility at the Research Institute for Sustainable Humanosphere, Kyoto University. This research was partially supported by the Research Support Project for Life Science and Drug Discovery (Basis for Supporting Innovative Drug Discovery and Life Science Research [BINDS]) from AMED under grant number JP22ama 121003. The cryo-EM experiments for data collection were performed with the approval of the SPring-8 Proposal Review Committee (2021B2538, 2022A2538, 2022A2747, 2022B2747, 2023A2738, and 2023B2738). This work was supported by JSPS KAKENHI grant numbers 21K07024 and 24K10218 (to K.K.), 20K16245 and 23K14519 (to H.O.), 24KJ1623 (to M.I.). This work was conducted as part of "The Nippon Foundation - Osaka University Project for Infectious Disease Prevention." This work was also supported by AMED under grant number JP223fa627002 (to S.N.).

AUTHOR CONTRIBUTIONS

K.K., resources, data curation, formal analysis, validation, investigation, visualization, methodology, writing—original draft, and writing—review and editing; H.O., resources, data curation, formal analysis, validation, investigation, visualization, methodology, writing—original draft, and writing—review and editing; M.I., resources, data curation, formal analysis, validation, investigation, visualization, and methodology; R.M., resources, data curation, formal analysis, validation, investigation, visualization, and methodology; T. Imai, data curation, formal analysis, validation, investigation, visualization, methodology, and writing—review and editing; C.G., data curation, formal analysis, validation, investigation, visualization, methodology, and writing—review and editing; H.S., data curation, formal analysis, validation, investigation, visualization, methodology, and writing—review and editing; S.M., data curation, formal analysis, validation, investigation, visualization, methodology, and writing—review and editing; T. Iida, data curation, formal analysis, validation, investigation, visualization, methodology, and writing—review and editing; S.N., resources, data curation, formal analysis, validation, investigation, visualization, methodology, writing—original draft, and writing—review and editing.

DECLARATION OF INTERESTS

The authors declare no competing interests.

STAR★METHODS

Detailed methods are provided in the online version of this paper and include the following:

- KEY RESOURCES TABLE
- EXPERIMENTAL MODEL AND STUDY PARTICIPANT DETAILS
  - Bacterial strain
- METHOD DETAILS
  - Pili purification
  - Negative-staining transmission electron microscopy
  - Cryo-EM data collection
  - Cryo-EM image processing for CFA/III filament
  - Model building and refinement of CFA/III filament
  - Cryo-EM image processing for the FimA filament
  - Model building and refinement of the FimA filament
  - Genome sequencing and assembly of ETEC strain 31-10
- QUANTIFICATION AND STATISTICAL ANALYSIS

SUPPLEMENTAL INFORMATION

Supplemental information can be found online at https://doi.org/10.1016/j.str.2025.03.010.

Received: December 25, 2024
Revised: February 18, 2025
Accepted: March 18, 2025
Published: April 11, 2025

REFERENCES

1. Edwards, R.A., and Puente, J.L. (1998). Fimbrial expression in enteric bacteria: A critical step in intestinal pathogenesis. Trends Microbiol. *6*, 282–287. https://doi.org/10.1016/s0966-842x(98)01288-8.
2. Kline, K.A., Fälker, S., Dahlberg, S., Normark, S., and Henriques-Normark, B. (2009). Bacterial adhesins in host–microbe interactions. Cell Host Microbe *5*, 580–592. https://doi.org/10.1016/j.chom.2009.05.011.
3. Hospenthal, M.K., Costa, T.R.D., and Waksman, G. (2017). A comprehensive guide to pilus biogenesis in Gram-negative bacteria. Nat. Rev. Microbiol. *15*, 365–379. https://doi.org/10.1038/nrmicro.2017.40.
4. Madhavan, T.P.V., and Sakellaris, H. (2015). Colonization factors of enterotoxigenic Escherichia coli. Adv. Appl. Microbiol. *90*, 155–197. https://doi.org/10.1016/bs.aambs.2014.09.003.
5. Waksman, G., and Hultgren, S.J. (2009). Structural biology of the chaperone-usher pathway of pilus biogenesis. Nat. Rev. Microbiol. *7*, 765–774. https://doi.org/10.1038/nrmicro2220.
6. Craig, L., Pique, M.E., and Tainer, J.A. (2004). Type IV pilus structure and bacterial pathogenicity. Nat. Rev. Microbiol. *2*, 363–378. https://doi.org/10.1038/nrmicro885.
7. Craig, L., Forest, K.T., and Maier, B. (2019). Type IV pili: Dynamics, biophysics and functional consequences. Nat. Rev. Microbiol. *17*, 429–440. https://doi.org/10.1038/s41579-019-0195-4.
8. Pelicic, V. (2023). Mechanism of assembly of type 4 filaments: Everything you always wanted to know (but were afraid to ask). Microbiology (Read.) *169*, 001311. https://doi.org/10.1099/mic.0.001311.
9. Giltner, C.L., Nguyen, Y., and Burrows, L.L. (2012). Type IV pilin proteins: Versatile molecular modules. Microbiol. Mol. Biol. Rev. *76*, 740–772. https://doi.org/10.1128/MMBR.00035-12.
10. Wizemann, T.M., Adamou, J.E., and Langermann, S. (1999). Adhesins as targets for vaccine development. Emerg. Infect. Dis. *5*, 395–403. https://doi.org/10.3201/eid0503.990310.
11. Steadman, D., Lo, A., Waksman, G., and Remaut, H. (2014). Bacterial surface appendages as targets for novel antibacterial therapeutics. Future Microbiol. *9*, 887–900. https://doi.org/10.2217/fmb.14.46.
12. Rasko, D.A., and Sperandio, V. (2010). Anti-virulence strategies to combat bacteria-mediated disease. Nat. Rev. Drug Discov. *9*, 117–128. https://doi.org/10.1038/nrd3013.
13. Egelman, E.H. (2017). Cryo-EM of bacterial pili and archaeal flagellar filaments. Curr. Opin. Struct. Biol. *46*, 31–37. https://doi.org/10.1016/j.sbi.2017.05.012.
14. Garnett, J.A., and Atherton, J. (2021). Structure determination of microtubules and pili: past, present, and future directions. Front. Mol. Biosci. *8*, 830304. https://doi.org/10.3389/fmolb.2021.830304.
15. Craig, L., Volkmann, N., Arvai, A.S., Pique, M.E., Yeager, M., Egelman, E.H., and Tainer, J.A. (2006). Type IV pilus structure by cryo-electron microscopy and crystallography: Implications for pilus assembly and functions. Mol. Cell *23*, 651–662. https://doi.org/10.1016/j.molcel.2006.07.004.
16. Li, J., Egelman, E.H., and Craig, L. (2012). Structure of the *Vibrio cholerae* type IVb Pilus and stability comparison with the *Neisseria gonorrhoeae* type IVa pilus. J. Mol. Biol. *418*, 47–64. https://doi.org/10.1016/j.jmb.2012.02.017.

17. Kolappan, S., Coureuil, M., Yu, X., Nassif, X., Egelman, E.H., and Craig, L. (2016). Structure of the *Neisseria meningitidis* type IV pilus. Nat. Commun. *7*, 13015. https://doi.org/10.1038/ncomms13015.

18. Wang, F., Coureuil, M., Osinski, T., Orlova, A., Altindal, T., Gesbert, G., Nassif, X., Egelman, E.H., and Craig, L. (2017). Cryoelectron microscopy reconstructions of the *Pseudomonas aeruginosa* and *Neisseria gonorrhoeae* type IV pili at sub-nanometer resolution. Structure *25*, 1423–1435.e4. https://doi.org/10.1016/j.str.2017.07.016.

19. Bardiaux, B., de Amorim, G.C., Luna Rico, A., Zheng, W., Guilvout, I., Jollivet, C., Nilges, M., Egelman, E.H., Izadi-Pruneyre, N., and Francetic, O. (2019). Structure and assembly of the enterohemorrhagic Escherichia coli type 4 Pilus. Structure *27*, 1082–1093.e5. https://doi.org/10.1016/j.str.2019.03.021.

20. Hospenthal, M.K., Zyla, D., Costa, T.R.D., Redzej, A., Giese, C., Lillington, J., Glockshuber, R., and Waksman, G. (2017). The cryoelectron microscopy structure of the type 1 chaperone-usher pilus rod. Structure *25*, 1829–1838.e4. https://doi.org/10.1016/j.str.2017.10.004.

21. Spaulding, C.N., Schreiber, H.L., Zheng, W., Dodson, K.W., Hazen, J.E., Conover, M.S., Wang, F., Svenmarker, P., Luna-Rico, A., Francetic, O., et al. (2018). Functional role of the type 1 pilus rod structure in mediating host–pathogen interactions. Elife *7*, e31662. https://doi.org/10.7554/eLife.31662.

22. Neuhaus, A., Selvaraj, M., Salzer, R., Langer, J.D., Kruse, K., Kirchner, L., Sanders, K., Daum, B., Averhoff, B., and Gold, V.A.M. (2020). Cryo-electron microscopy reveals two distinct type IV pili assembled by the same bacterium. Nat. Commun. *11*, 2231. https://doi.org/10.1038/s41467-020-15650-w.

23. Sonani, R.R., Sanchez, J.C., Baumgardt, J.K., Kundra, S., Wright, E.R., Craig, L., and Egelman, E.H. (2023). Tad and toxin-coregulated pilus structures reveal unexpected diversity in bacterial type IV pili. Proc. Natl. Acad. Sci. USA *120*, e2316668120. https://doi.org/10.1073/pnas.2316668120.

24. Treuner-Lange, A., Zheng, W., Viljoen, A., Lindow, S., Herfurth, M., Dufrêne, Y.F., Søgaard-Andersen, L., and Egelman, E.H. (2024). Tight-packing of large pilin subunits provides distinct structural and mechanical properties for the *Myxococcus xanthus* type IVa pilus. Proc. Natl. Acad. Sci. USA *121*, e2321989121. https://doi.org/10.1073/pnas.2321989121.

25. Doran, M.H., Baker, J.L., Dahlberg, T., Andersson, M., and Bullitt, E. (2023). Three structural solutions for bacterial adhesion pilus stability and superelasticity. Structure *31*, 529–540.e7. https://doi.org/10.1016/j.str.2023.03.005.

26. Evans, D.G., Evans, D.J., and Tjoa, W. (1977). Hemagglutination of human group A erythrocytes by enterotoxigenic Escherichia coli isolated from adults with diarrhea: Correlation with colonization factor. Infect. Immun. *18*, 330–337. https://doi.org/10.1128/iai.18.2.330-337.1977.

27. Kawahara, K., Oki, H., Fukakusa, S., Yoshida, T., Imai, T., Maruno, T., Kobayashi, Y., Motooka, D., Iida, T., Ohkubo, T., and Nakamura, S. (2016). Homo-trimeric structure of the type IVb minor pilin CofB suggests mechanism of CFA/III pilus assembly in human enterotoxigenic Escherichia coli. J. Mol. Biol. *428*, 1209–1226. https://doi.org/10.1016/j.jmb.2016.02.003.

28. Oki, H., Kawahara, K., Maruno, T., Imai, T., Muroga, Y., Fukakusa, S., Iwashita, T., Kobayashi, Y., Matsuda, S., Kodama, T., et al. (2018). Interplay of a secreted protein with type IVb pilus for efficient enterotoxigenic Escherichia coli colonization. Proc. Natl. Acad. Sci. USA *115*, 7422–7427. https://doi.org/10.1073/pnas.1805671115.

29. Taniguchi, T., Akeda, Y., Haba, A., Yasuda, Y., Yamamoto, K., Honda, T., and Tochikubo, K. (2001). Gene cluster for assembly of pilus colonization factor antigen III of enterotoxigenic Escherichia coli. Infect. Immun. *69*, 5864–5873. https://doi.org/10.1128/IAI.69.9.5864-5873.2001.

30. Kolappan, S., Roos, J., Yuen, A.S.W., Pierce, O.M., and Craig, L. (2012). Structural characterization of CFA/III and longus type IVb Pili from enterotoxigenic Escherichia coli. J. Bacteriol. *194*, 2725–2735. https://doi.org/10.1128/JB.00282-12.

31. Punjani, A., Rubinstein, J.L., Fleet, D.J., and Brubaker, M.A. (2017). cryoSPARC: Algorithms for rapid unsupervised cryo-EM structure determination. Nat. Methods *14*, 290–296. https://doi.org/10.1038/nmeth.4169.

32. Jamali, K., Käll, L., Zhang, R., Brown, A., Kimanius, D., and Scheres, S.H.W. (2024). Automated model building and protein identification in cryo-em maps. Nature *628*, 450–457. https://doi.org/10.1038/s41586-024-07215-4.

33. Oki, H., Kawahara, K., Iimori, M., Imoto, Y., Nishiumi, H., Maruno, T., Uchiyama, S., Muroga, Y., Yoshida, A., Yoshida, T., et al. (2022). Structural basis for the toxin-coregulated pilus-dependent secretion of *Vibrio cholerae* colonization factor. Sci. Adv. *8*, eabo3013. https://doi.org/10.1126/sciadv.abo3013.

34. Roux, N., Spagnolo, J., and de Bentzmann, S. (2012). Neglected but amazingly diverse type IVb pili. Res. Microbiol. *163*, 659–673. https://doi.org/10.1016/j.resmic.2012.10.015.

35. Denise, R., Abby, S.S., and Rocha, E.P.C. (2019). Diversification of the type IV filament superfamily into machines for adhesion, protein secretion, DNA uptake, and motility. PLoS Biol. *17*, e3000390. https://doi.org/10.1371/journal.pbio.3000390.

36. Fukakusa, S., Kawahara, K., Nakamura, S., Iwashita, T., Baba, S., Nishimura, M., Kobayashi, Y., Honda, T., Iida, T., Taniguchi, T., and Ohkubo, T. (2012). Structure of the CFA/III major pilin subunit CofA from human enterotoxigenic Escherichia coli determined at 0.90 Å resolution by sulfur-SAD phasing. Acta Crystallogr. D Biol. Crystallogr. *68*, 1418–1429. https://doi.org/10.1107/S0907444912034464.

37. Parge, H.E., Forest, K.T., Hickey, M.J., Christensen, D.A., Getzoff, E.D., and Tainer, J.A. (1995). Structure of the fibre-forming protein pilin at 2.6 A resolution. Nature *378*, 32–38. https://doi.org/10.1038/378032a0.

38. Craig, L., Taylor, R.K., Pique, M.E., Adair, B.D., Arvai, A.S., Singh, M., Lloyd, S.J., Shin, D.S., Getzoff, E.D., Yeager, M., et al. (2003). Type IV pilin structure and assembly: X-ray and EM analyses of *Vibrio cholerae* toxin-coregulated pilus and *Pseudomonas aeruginosa* PAK pilin. Mol. Cell *11*, 1139–1150. https://doi.org/10.1016/s1097-2765(03)00170-9.

39. Hartung, S., Arvai, A.S., Wood, T., Kolappan, S., Shin, D.S., Craig, L., and Tainer, J.A. (2011). Ultrahigh resolution and full-length pilin structures with insights for filament assembly, pathogenic functions, and vaccine potential. J. Biol. Chem. *286*, 44254–44265. https://doi.org/10.1074/jbc.M111.297242.

40. Reynolds, M.J., Hachicho, C., Carl, A.G., Gong, R., and Alushin, G.M. (2022). Bending forces and nucleotide state jointly regulate F-actin structure. Nature *611*, 380–386. https://doi.org/10.1038/s41586-022-05366-w.

41. Li, J., Lim, M.S., Li, S., Brock, M., Pique, M.E., Woods, V.L., Jr., and Craig, L. (2008). *Vibrio cholerae* toxin-coregulated pilus structure analyzed by hydrogen/deuterium exchange mass spectrometry. Structure *16*, 137–148. https://doi.org/10.1016/j.str.2007.10.027.

42. Sheikh, A., Rashu, R., Begum, Y.A., Kuhlman, F.M., Ciorba, M.A., Hultgren, S.J., Qadri, F., and Fleckenstein, J.M. (2017). Highly conserved type 1 pili promote enterotoxigenic *E. coli* pathogen–host interactions. PLoS Neglected Trop. Dis. *11*, e0005586. https://doi.org/10.1371/journal.pntd.0005586.

43. Cumsille, A., Durán, R.E., Rodríguez-Delherbe, A., Saona-Urmeneta, V., Cámara, B., Seeger, M., Araya, M., Jara, N., and Buil-Aranda, C. (2023). GenoVi, an open-source automated circular genome visualizer for bacteria and archaea. PLoS Comput. Biol. *19*, e1010998. https://doi.org/10.1371/journal.pcbi.1010998.

44. Jurrus, E., Engel, D., Star, K., Monson, K., Brandi, J., Felberg, L.E., Brookes, D.H., Wilson, L., Chen, J., Liles, K., et al. (2018). Improvements to the APBS biomolecular solvation software suite. Protein Sci. *27*, 112–128. https://doi.org/10.1002/pro.3280.

45. Santos-Moreno, J., East, A., Guilvout, I., Nadeau, N., Bond, P.J., Tran Van Nhieu, G., and Francetic, O. (2017). Polar N-terminal residues conserved in type 2 secretion pseudopilins determine subunit targeting and membrane extraction steps during fibre assembly. J. Mol. Biol. *429*, 1746–1765. https://doi.org/10.1016/j.jmb.2017.04.005.

46. Nivaskumar, M., Santos-Moreno, J., Malosse, C., Nadeau, N., Chamot-Rooke, J., Tran Van Nhieu, G., and Francetic, O. (2016). Pseudopilin

residue E5 is essential for recruitment by the type 2 secretion system assembly platform. Mol. Microbiol. *101*, 924–941. https://doi.org/10.1111/mmi.13432.

47. Chlebek, J.L., Denise, R., Craig, L., and Dalia, A.B. (2021). Motor-independent retraction of type IV pili is governed by an inherent property of the pilus filament. Proc. Natl. Acad. Sci. USA *118*, e2102780118. https://doi.org/10.1073/pnas.2102780118.

48. Biais, N., Higashi, D.L., Brujic, J., So, M., and Sheetz, M.P. (2010). Force-dependent polymorphism in type IV pili reveals hidden epitopes. Proc. Natl. Acad. Sci. USA *107*, 11358–11363. https://doi.org/10.1073/pnas.0911328107.

49. Armstrong, M., Han, B.-G., Gomez, S., Turner, J., Fletcher, D.A., and Glaeser, R.M. (2020). Microscale fluid behavior during cryo-EM sample blotting. Biophys. J. *118*, 708–719. https://doi.org/10.1016/j.bpj.2019.12.017.

50. Stachowski, T.R., Vanarotti, M., Seetharaman, J., Lopez, K., and Fischer, M. (2022). Water networks repopulate protein-ligand interfaces with temperature. Angew. Chem. Int. Ed. Engl. *61*, e202112919. https://doi.org/10.1002/anie.202112919.

51. Mastronarde, D.N. (2003). SerialEM: A program for automated tilt series acquisition on Tecnai microscopes using prediction of specimen position. Microsc. Microanal. *9*, 1182–1183. https://doi.org/10.1017/S1431927603445911.

52. Emsley, P., and Cowtan, K. (2004). Coot: Model-building tools for molecular graphics. Acta Crystallogr. D Biol. Crystallogr. *60*, 2126–2132. https://doi.org/10.1107/S0907444904019158.

53. Afonine, P.V., Poon, B.K., Read, R.J., Sobolev, O.V., Terwilliger, T.C., Urzhumtsev, A., and Adams, P.D. (2018). Real-space refinement in PHENIX for cryo-EM and crystallography. Acta Crystallogr. D Struct. Biol. *74*, 531–544. https://doi.org/10.1107/S2059798318006551.

54. Williams, C.J., Headd, J.J., Moriarty, N.W., Prisant, M.G., Videau, L.L., Deis, L.N., Verma, V., Keedy, D.A., Hintze, B.J., Chen, V.B., et al. (2018). MolProbity: More and better reference data for improved all-atom structure validation. Protein Sci. *27*, 293–315. https://doi.org/10.1002/pro.3330.

55. Kolmogorov, M., Yuan, J., Lin, Y., and Pevzner, P.A. (2019). Assembly of long, error-prone reads using repeat graphs. Nat. Biotechnol. *37*, 540–546. https://doi.org/10.1038/s41587-019-0072-8.

56. Li, H. (2018). Minimap2: Pairwise alignment for nucleotide sequences. Bioinformatics *34*, 3094–3100. https://doi.org/10.1093/bioinformatics/bty191.

57. Walker, B.J., Abeel, T., Shea, T., Priest, M., Abouelliel, A., Sakthikumar, S., Cuomo, C.A., Zeng, Q., Wortman, J., Young, S.K., and Earl, A.M. (2014). Pilon: An integrated tool for comprehensive microbial variant detection and genome assembly improvement. PLoS One *9*, e112963. https://doi.org/10.1371/journal.pone.0112963.

58. Tanizawa, Y., Fujisawa, T., and Nakamura, Y. (2018). DFAST: A flexible prokaryotic genome annotation pipeline for faster genome publication. Bioinformatics *34*, 1037–1039. https://doi.org/10.1093/bioinformatics/btx713.

59. Pettersen, E.F., Goddard, T.D., Huang, C.C., Meng, E.C., Couch, G.S., Croll, T.I., Morris, J.H., and Ferrin, T.E. (2021). UCSF ChimeraX: Structure visualization for researchers, educators, and developers. Protein Sci. *30*, 70–82. https://doi.org/10.1002/pro.3943.

STAR★METHODS

KEY RESOURCES TABLE

REAGENT or RESOURCE	SOURCE	IDENTIFIER
Bacterial and virus strains		
Enterotoxigenic *Escherichia coli* strain 31-10	Taniguchi et al.[29]	N/A
Chemicals, peptides, and recombinant proteins		
LB Broth	Nacalai tesque	20068-75
Casamino acids	Gibco	223050
Yeast extract	Gibco	211929
Agar	Nacalai tesque	01028-85
Deposited data		
Cryo-EM map of CFA/III	This paper	EMDB:EMD-60902
Atomic coordinates of CFA/III	This paper	PDB:9IUF
Cryo-EM map of type I pilus	This paper	EMDB:EMD-60903
Atomic coordinates of type I pilus	This paper	PDB:9IUG
Sequencing data of ETEC strain 31-10	This paper	DDBJ:PRJDB18453
Software and algorithms		
CryoSPARC v4.5.3.	Punjani et al.[31]	https://cryosparc.com/docs
ModelAngelo	Jamali et al.[32]	https://github.com/3dem/model-angelo
GenoVi	Cumsille et al.[43]	https://github.com/robotoD/GenoVi
Adaptive Poisson-Boltzmann Solver (APBS)	Jurrus et al.[44]	https://server.poissonboltzmann.org/
Serial EM	Mastronarde, D.N.[51]	N/A
Coot	Emsley et al.[52]	https://www2.mrc-lmb.cam.ac.uk/personal/pemsley/coot/
PHENIX	Afonine et al.[53]	https://phenix-online.org/
MolProbity	Williams et al.[54]	https://phenix-online.org/documentation/tutorials/molprobity.html
Flye 2.9.4	Kolomogorov et al.[55]	https://github.com/mikolmogorov/Flye
medaka v1.12.0	Oxford Nanopore Technologies	https://github.com/nanoporetech/medaka/releases
minimap2 v2.28	Li et al.[56]	https://github.com/lh3/minimap2
pilon v1.24	Walker et al.[57]	https://github.com/broadinstitute/pilon/releases/
DFAST	Tanizawa et al.[58]	https://dfast.ddbj.nig.ac.jp/
PyMOL	Schrodinger, LLC	https://www.pymol.org/
ChimeraX	Pettersen et al.[59]	https://www.cgl.ucsf.edu/chimerax/

EXPERIMENTAL MODEL AND STUDY PARTICIPANT DETAILS

Bacterial strain

Enterotoxigenic *Escherichia coli* (ETEC) strain 31-10[29] was used in this study.

METHOD DETAILS

Pili purification

ETEC strain 31-10,[29] pre-cultured in LB medium at 20°C, was applied to a CFA agar plate (1% casamino acids, 0.15% yeast extract, 0.005% $MgSO_4$, 0.0005% $MnCl_2$, and 2% agar)[26] and incubated at 37°C to induce the expression of CFs. The cultured bacteria were collected in phosphate-buffered Saline (PBS) containing 5 mM EDTA, and the expressed bacterial filaments were harvested by vortexing. After centrifugation twice at 8,000 × *g* and 4°C for 30 min, to remove the bacterial debris, ammonium sulfate was added to 30% saturation to the supernatant to precipitate the filaments. The precipitate was dissolved in PBS and dialyzed to remove any remaining ammonium sulfate. For further purification of bacterial filaments, such as CFA/III, we performed density gradient

centrifugation at 100,000 × *g* and 4°C for 3 h using 10%–50% (w/v) sucrose. Ultracentrifugation separated an upper layer containing *E. coli* proteins, a middle layer containing bacterial filaments, and a lower layer containing bacterial debris. The middle layer contains a major pilin CofA of CFA/III, as determined through SDS-PAGE analysis of the fraction.

Negative-staining transmission electron microscopy

The purified filament fraction was concentrated to approximately 0.3 mg/ml. The filament fraction (2.5 μl) was incubated at 8°C for 5 min and applied onto a glow-discharged carbon-coated copper grid, and then washed with two droplets of buffer (50 mM Tris-HCl, 150 mM NaCl, pH 7.4) prior to negative staining with 1% uranyl acetate. The prepared mesh was observed using a JEM-1400 (JEOL Ltd.) operated at 120 kV accelerating voltage and recorded using the built-in CCD camera.

Cryo-EM data collection

The purified filament fraction was dialyzed against buffer (20 mM Tris-HCl, 150 mM NaCl, pH 8.0) and concentrated to approximately 3 mg/ml for cryo-EM data collection. A purified filament fraction (2 μl) was applied to a copper grid (R1.2/1.3 300 mesh; Quantifoil) and glow-discharged for 10 s using a JEC-3000FC Auto Fine Coater (JEOL). The grid was blotted for 3 s at 8°C (100% humidity) using a blot force of 10 and then plunge-frozen in liquid ethane using a Vitrobot Mark IV System (Thermo Fisher Scientific). Screening and data collections were conducted using a CRYO ARM™ 200 or 300 electron microscope (JEOL) operating at 200 or 300 kV, equipped with a cold field-emission gun, an in-column Omega energy filter (20 eV slit width), and a K2 or K3 direct electron detector (Gatan), respectively. For screening, we used the customizable automated data acquisition system JADAS (JEOL), whereas cryo-EM movies for data collection were acquired using the automated EM data acquisition program Serial EM[51] with 5 × 5 beam-image shift patterns (coma *vs.* image shift calibration was performed prior to data acquisition). A total of 6,899 movies were collected on a CRYO ARM™ 300 electron microscope (JEOL) using a nominal magnification of ×60,000 at a pixel size of 0.752 Å/pixel. Each movie was divided into 50 frames using a total dose of 53.77 e^{-}/Å^2, with the K3 detector operating in the correlated double-sampling (CDS) mode. All parameters involved in data collection are presented in Table S1.

Cryo-EM image processing for CFA/III filament

All data processing of cryo-EM movies obtained in this study was performed using CryoSPARC v4.5.3.[31] The imported movies were first subjected to beam-induced motion correction by using the function "Patch motion correction," and the CTF parameters were assessed using "Patch CTF estimation." We manually picked hundreds of non-overlapping filament segments and performed 2D classification. Selected 2D classes were then used as templates to trace the helical filament found in all the micrographs using the program "Filament Tracer", and a total of 3,011,705 particles were extracted using a box size of 300 Å. Subsequent 2D classification results in a well-resolved 2D class image that shows a feature corresponding to the T4P filament. A total of 2,887,506 particles were selected for further data processing. We initially calculated the helical volume by "Helical Refinement" without the input of any helical symmetry parameter, and then searched for helical parameters by the "Symmetry Search Utility", with previously estimated values of an axial rise of 8.5 Å and a twist angle of 96.8° from the negative-staining reconstruction of TCP from *V. cholerae* as a reference,[16] revealed that the volume has a helical rise of 8.01 Å and twist angle of 94.63°. The parameter set was used for "Helical Refinement" that led to a map of 2.1 Å resolution. After local and global CTF refinement, each particle was motion-corrected with "Reference Based Motion Correction" and high-quality particles were then selected by 2D and 3D classification. After further local and global CTF refinement, "Helical Refinement" using 1,425,921 particles yielded a volume with a helical rise of 8.01 Å, a twist angle of 94.55°, and a resolution of 1.8 Å, based on the "gold-standard" map:map FSC criterion of 0.143. The image processing workflow for the CFA/III reconstruction is shown in Figure S2, and the map:map and model map FSC curves are shown in Figure S3.

Model building and refinement of CFA/III filament

The initial model of the CFA/III filament was automatically built into the cryo-EM density map using ModelAngelo,[32] initially without using any sequence input and then using the sequence of major pilin CofA (GenBank code: BAB62897.1).[29] The model was manually refined using the program Coot[52] and subjected to a real-space refinement using phenixsu.real_space_refine implemented in PHENIX.[53] During manual model building using Coot, we observed an alternative conformation of Met1 at lower contour level for both original and sharpened map (at 1.5 and 2.0 RMSD, respectively), in addition to one that directs its N-terminal amine toward the side chain of Glu5 to form an electrostatic interaction (Figure 2D). The residual density shows that the N-terminal amine is positioned to interact with surrounding hydrophobic residues of neighboring subunits, suggesting its methylation.[9] However, due to its low occupancy, we did not include this conformation in the final model. Water molecules were automatically located with a criterion of density level (more than 1.5 RMSD) in the original map using Coot and then manually checked. The geometries of the CFA/III filament model were verified using MolProbity.[54] All refinement statistics are listed in Table S1. Figures were prepared using PyMOL (https://www.pymol.org) or ChimeraX (https://www.cgl.ucsf.edu/chimerax).[59]

Cryo-EM image processing for the FimA filament

Since there are a small number of filaments in the cryo-EM micrographs that apparently have morphology different from CFA/III, we also performed reconstruction of such filaments. The particle picking was done by using the program "Filament Tracer" with a filament diameter of 65 Å. The 2D classification of extracted images suggests that the observed filaments have a feature reminiscent of CUP. The selected 2D classes were then used as templates to trace the filament using the "Filament Tracer". The filament images

observed in all of the cryo-EM micrographs were further segmented into 10,097,033 particles using a box size of 300 Å. After several rounds of 2D classification, 48,324 particles were selected and used in generating an initial helical volume. The search for helical parameters using the "Symmetry Search Utility", with previously estimated values of an axial rise of 8.0 Å and a twist angle of 115° for T1P as a reference, revealed that the helical volume has helical parameters with a helical rise of 7.72 Å and twist angle of 114.90°. After local and global CTF refinement and motion correction with "Reference Based Motion Correction", high-quality particles were selected by 2D classification. After further local and global CTF refinement, the helical refinement using 43,184 particles yielded a well-resolved volume map amenable to model the T1P as detailed below with a helical rise of 7.71 Å, twist angle of 114.95°, and resolution of 2.2 Å, based on the "gold-standard" map:map FSC criterion of 0.143. The image processing workflow for the T1P filament reconstruction is shown in Figure S5, and the map:map and model map FSC curves are shown in Figure S6.

Model building and refinement of the FimA filament

The initial model was automatically built into the cryo-EM density map using ModelAngelo,[32] without using any sequence input. The modeling estimates the subunit sequence, which has 84% sequence identity with the sequences of the type I fimbrial subunit protein FimA from *Shigella flexneri* and ETEC (GenBank code: UMV06456.1 and QED7455.1, respectively) from UPEC. Since no FimA sequence for ETEC strain 31-10 had been reported, we determined the sequence here (as described below) and then used it for further model building by ModelAngelo.[32] The model was manually refined using the program Coot[52] and then subjected to a real-space refinement using "phenix.real_space_refine" implemented in PHENIX.[53] Water molecules were automatically located with criteria of density level (more than 1.5 RMSD) in the original map using Coot,[52] and then manually checked. The geometries of the FimA filament model were verified using MolProbity.[54] All refinement statistics are listed in Table S1. Figures were prepared using PyMOL (https://www.pymol.org) or ChimeraX (https://www.cgl.ucsf.edu/chimerax).[59]

Genome sequencing and assembly of ETEC strain 31-10

The ETEC strain 31-10 was cultured in LB medium at 25°C, and cell pellets were collected by centrifugation. Bacterial DNA was extracted from the precipitation using the DNeasy PowerSoil Kit (QIAGEN). The extracted bacterial genomic DNA was sequenced using both short and long-read sequencing platforms. Short read sequencing by MiSeq (Illumina) was performed using the KAPA Hyper Plus Library Preparation Kit (Kapa Biosystems) in a 2 × 151 bp paired-end run. Long-read sequencing data was obtained using MinION (Oxford Nanopore Technologies) sequencing with the Ligation Sequencing Kit SQK-LSK109 (Oxford Nanopore Technologies). Long-read data were assembled using Flye software v2.9.4,[55] resulting in three contigs corresponding to one chromosome and two plasmids. The assembled data were corrected using medaka software v1.12.0 (https://github.com/nanoporetech/medaka) and then minimap2 v2.28[56] and pilon v1.24[57] utilizing short-read sequencing data. We annotated the genome of ETEC strain 31-10 using DFAST.[58]

QUANTIFICATION AND STATISTICAL ANALYSIS

Cryo-EM data collection and refinement statistics are summarized in Table S1.